

A direct probe of cosmological power spectra of the peculiar velocity field and the gravitational lensing magnification from photometric redshift surveys

Adi Nusser,^{a,b} Enzo Branchini,^{c,d,e} and Martin Feix^a

^aDepartment of Physics, Israel Institute of Technology - Technion, Haifa 32000, Israel

^bAsher Space Science Institute, Israel Institute of Technology - Technion, Haifa 32000, Israel

^cDepartment of Physics, Università Roma Tre, Via della Vasca Navale 84, Rome 00146, Italy

^dINFN Sezione di Roma 3, Via della Vasca Navale 84, Rome 00146, Italy

^eINAF, Osservatorio Astronomico di Brera, Via Brera 28, Milano 20121, Italy

E-mail: adi@physics.technion.ac.il, branchin@fis.uniroma3.it,
mfeix@physics.technion.ac.il

Abstract. The cosmological peculiar velocity field (deviations from the pure Hubble flow) of matter carries significant information on dark energy, dark matter and the underlying theory of gravity on large scales. Peculiar motions of galaxies introduce systematic deviations between the observed galaxy redshifts z and the corresponding cosmological redshifts z_{cos} . A novel method for estimating the angular power spectrum of the peculiar velocity field based on observations of galaxy redshifts and apparent magnitudes m (or equivalently fluxes) is presented. This method exploits the fact that a mean relation between z_{cos} and m of galaxies can be derived from all galaxies in a redshift-magnitude survey. Given a galaxy magnitude, it is shown that the $z_{\text{cos}}(m)$ relation yields its cosmological redshift with a 1σ error of $\sigma_z \sim 0.3$ for a survey like Euclid ($\sim 10^9$ galaxies at $z \lesssim 2$), and can be used to constrain the angular power spectrum of $z - z_{\text{cos}}(m)$ with a high signal-to-noise ratio. At large angular separations corresponding to $l \lesssim 15$, we obtain significant constraints on the power spectrum of the peculiar velocity field. At $15 \lesssim l \lesssim 60$, magnitude shifts in the $z_{\text{cos}}(m)$ relation caused by gravitational lensing magnification dominate, allowing us to probe the line-of-sight integral of the gravitational potential. Effects related to the environmental dependence in the luminosity function can easily be computed and their contamination removed from the estimated power spectra. The amplitude of the combined velocity and lensing power spectra at $z \sim 1$ can be measured with $\lesssim 5\%$ accuracy.

Keywords: dark matter and dark energy, large-scale structure of the Universe, redshift surveys, power spectrum

ArXiv ePrint: [1207.5800](https://arxiv.org/abs/1207.5800)

1 Introduction

Dark matter, dark energy, and the theory of gravitation dictate the evolution of large-scale structure in the Universe. The physical conditions allowing for the formation of galaxies, ultimately lead to a bias between the distribution of galaxies and the underlying mass density. However, large-scale motions of galaxies are most certainly locked to the peculiar velocity field associated with the gravitational tug of the total underlying mass fluctuations. This assumes that gravity is the only relevant large-scale force and neglects the contribution from decaying linear modes. Despite the bias between the distribution of galaxies and the underlying matter field, the clustering properties of galaxies have been the main tool for testing cosmological models. Currently planned galaxy surveys will allow us to quantify the clustering of galaxies on hundreds of comoving Mpc and to even measure coherent distortions of galaxy images which arise from gravitational lensing by the foreground matter.

On the other hand, the peculiar motions of galaxies have traditionally been less successful as a cosmological tool, and there are several reasons for that. Neglecting other potentially important effects (see section 2 for details), peculiar velocities are approximately equal to the redshifts less the corresponding Hubble expansion recession velocities. The latter require direct measurements of galaxy distances which are available for only a small fraction of galaxies. Presently, the number of galaxies with measured distances is several orders of magnitude below that of galaxies in redshift surveys used for clustering studies. Furthermore, although the underlying peculiar velocity is an honest tracer of the general matter flow, the inference of peculiar velocities from observational data is plagued with observational biases [1]. Traditional peculiar velocity catalogs are expected to improve within the next few years, but it remains questionable how well observational biases will be controlled, especially at large distances. An alternative probe of the peculiar velocity field may be astrometric measurements of galaxies by the Gaia space mission [2, 3]. This probe is essentially free of the classic biases contaminating traditional peculiar velocity measurements, but it is also limited to nearby galaxies within $\sim 100h^{-1}$ Mpc.

Here we describe a method for deriving strong constraints on the power spectrum of the galaxies' peculiar velocity field independent of conventional direct distance measurements, which are prone to systematic errors, and any biasing relation between galaxies and mass. The method is an extension of the approaches we have recently proposed [4–6], and it relies on using the observed fluxes of galaxies as a proxy for their cosmological distance [7]. Although this most basic distance indicator is very noisy, the large number of galaxies available in future surveys will allow one to beat down this noise to a sufficiently low level. Planned galaxy redshift surveys such as Euclid [8, 9] will probe the structure of the Universe over thousands of (comoving) Mpc, comprising $\lesssim 10^8$ – 10^9 galaxies at $z \sim 1$ and beyond. These observations will provide redshifts and fluxes, z and f , respectively. The observed redshifts deviate from the cosmological redshifts which would be observed in a purely homogeneous universe. The large number of galaxies and the large sky coverage of these surveys can be used to derive a mean global relation between the mean redshift of a galaxy and its apparent magnitude $m = -2.5 \log f + \text{const}$. We interpret this relation as yielding the cosmological redshift $z_{\text{cos}}(m)$ for a given apparent magnitude m . Angular power spectra of the difference $z_i - z_{\text{cos}}(m_i)$ between the observed redshift z_i of a galaxy and its expected cosmological redshift z_{cos} should contain valuable information, mainly on the peculiar velocity field which is the main cosmological source for $z_i - z_{\text{cos}}(m_i)$. In this work, we will show that the velocity power spectrum on large scales of a few 100 Mpc could be constrained with significant

signal-to-noise ratio (S/N) at the effective depth of the survey. Another contribution to $z_i - z_{\text{cos}}(m_i)$ results from the time evolution of the gravitational potential along the photon path, but is significantly smaller than that induced by peculiar velocities as we will show below. There are two additional, indirect effects which modify the relation $z_{\text{cos}}(m)$ along a given line of sight. The first effect is related to the environmental dependence between galaxy luminosities and the large-scale structure in which they reside. Since this dependence is closely connected to the underlying density field, it can be self-consistently removed in our analysis. The second effect is caused by gravitational lensing magnification which changes the apparent magnitudes of galaxies in a given direction. This latter contribution could actually be very rewarding since gravitational lensing provides a direct probe of the underlying mass distribution. Considering the analysis presented below, we will therefore treat it as part of the sought signal.

The paper is structured as follows: We begin with a detailed description of the method and its application to galaxy redshift surveys in section 2. In section 3, we consider predictions for the standard Λ CDM model and discuss the method's viability as well as its expected performance. Finally, we present our conclusions in section 4. For clarity, some of the technical material is given separately in an appendix. In the following, we adopt the standard notation. The matter density and the cosmological constant in units of the critical density are denoted by Ω and Λ , respectively. The scale factor a is normalized to unity at the present time ($t = t_0$), and the Hubble function is defined as $H = \dot{a}/a$. Further, $r = c \int_t^{t_0} dt'/a(t')$ will be the comoving distance to an object and z its corresponding redshift, assuming a homogeneous and isotropic cosmological background. Throughout the paper, the subscript "0" will refer to quantities given at $t = t_0$, and a dot symbol denotes partial derivatives with respect to time t , i.e. $\dot{A} \equiv \partial A/\partial t$.

2 Methodology

In an inhomogeneous universe, the observed redshift z of a given object differs from its cosmological redshift z_{cos} (defined for the unperturbed background). The relative difference between these redshifts, $\Theta \equiv (z - z_{\text{cos}})/(1 + z_{\text{cos}})$, can be expressed as [10]

$$\Theta = \frac{V(t, r)}{c} - \frac{\Phi(t, r)}{c^2} - \frac{2}{c^2} \int_{t(r)}^{t_0} dt \frac{\partial \Phi[\hat{\mathbf{r}}r(t), t]}{\partial t}, \quad (2.1)$$

where $\hat{\mathbf{r}}$ is a unit vector along the line-of-sight to the object. Here the radial peculiar velocity V and the usual metric potential Φ are assumed as relative to their present-day values at $r = 0$ ($t = t_0$). The first and second terms on the right-hand side of eq. (2.1) are the Doppler and gravitational shifts, respectively, while the third term describes the energy change of light as it passes through a time-varying gravitational potential. Note that this third term is equivalent to the late-time integrated Sachs-Wolfe effect experienced by photons of the cosmic microwave background (CMB). In what follows, we will denote the three terms as Θ^V , Θ^Φ and $\Theta^{\dot{\Phi}}$, respectively. Also, we will consider angular power spectra (equivalent to angular correlations) of Θ on large scales where the corresponding signal is significant only relative to the expected error. Throughout this paper, we therefore rely on linear theory in a Λ CDM model where perturbations on all scales grow at the same rate. Introducing $D(t)$ as the growth rate of the underlying mass density contrast $\delta = \rho/\bar{\rho} - 1$, linear theory yields

the well-known relations

$$\delta(t, \mathbf{r}) = D(t)\delta_0(\mathbf{r}), \quad (2.2)$$

$$\Phi(\mathbf{r}, t) = \frac{D(t)}{a}\Phi_0(\mathbf{r}), \quad (2.3)$$

$$V(t, \mathbf{r}) = -\frac{2}{3}\frac{a\dot{D}(t)}{\Omega_0 H_0^2}\frac{\partial\Phi_0}{\partial r}, \quad (2.4)$$

where $D(t_0) = 1$. The second relation is obtained from the first using Poisson's equation, i.e. $\nabla_r^2\Phi = 3H_0^2\Omega_0\delta/2a$. For the special case $\Omega_0 = 1$, we have $D = a$ and fluctuations in the gravitational potential remain constant with time.

2.1 Cosmological redshift versus apparent magnitude

We aim to derive the field Θ sampled at the positions of all galaxies in a flux limited redshift survey covering a significant region of the sky together with a large number of galaxies. As an example, we consider the planned Euclid redshift survey [8, 9]. In order to obtain an estimate of Θ_i for each galaxy, we shall use apparent galaxy magnitudes (or equivalently fluxes) as a proxy to the cosmological redshift or distance. Although this most trivial distance indicator is very noisy, we will see that the high number of available galaxies allows one to beat down its scatter.

The mean cosmological redshift $z_{\text{cos}}(m)$ corresponding to a given apparent magnitude m is

$$z_{\text{cos}}(m) = \bar{z}_{\text{cos}} = \int_{z_1}^{z_2} z_{\text{cos}} P(z_{\text{cos}}|m) dz_{\text{cos}}, \quad (2.5)$$

and the root mean square (rms) scatter around this relation is

$$\sigma_z(m) = \int_{z_1}^{z_2} (z_{\text{cos}} - \bar{z}_{\text{cos}})^2 P(z_{\text{cos}}|m) dz_{\text{cos}}, \quad (2.6)$$

where z_1 and z_2 are the limiting redshifts in the survey, and $P(z_{\text{cos}}|m)$ denotes the probability that a galaxy with measured apparent magnitude m has a cosmological redshift z_{cos} . The $z_{\text{cos}}(m)$ relation can be linked to certain characteristics of the galaxy survey. The luminosity of a galaxy at z_{cos} is $L = 4\pi f d_L^2$ where $d_L(z_{\text{cos}})$ is the luminosity distance to the galaxy, and its absolute magnitude is defined as $M = -2.5 \log L + \text{const} = m - 5 \log d_L$. Let $\Phi(M)$ be the underlying luminosity function such that ΦdM is the number density of galaxies within the magnitude interval $[M, M + dM]$. Generally, the function $\Phi(M)$ depends on cosmic time, but in favor of a simplified description, we will assume for the moment that it varies little throughout the depth of the survey considered. Note that it is trivial to include a time-dependent evolutionary term in $\Phi(M)$. The probability $P(z_{\text{cos}}|m)$ satisfies

$$P(z_{\text{cos}}|m) \propto P(m|z_{\text{cos}})n(z_{\text{cos}}), \quad (2.7)$$

where $n(z_{\text{cos}})$ is the underlying mean number density of galaxies at z_{cos} . In the absence of galaxy population evolution, we have

$$n(z_{\text{cos}}) \propto d_c(z_{\text{cos}})^2 \frac{dd_c(z_{\text{cos}})}{dz_{\text{cos}}}, \quad (2.8)$$

where d_c is the comoving distance from the observer to z_{cos} . The relation in eq. (2.7) can be easily derived using Bayes' theorem which yields

$$P(z_{\text{cos}}|m)P(m) = P(m|z_{\text{cos}})P(z_{\text{cos}}), \quad (2.9)$$

where $P(m)$ can be directly estimated from observations, $P(z_{\text{cos}})$ is proportional to $n(z_{\text{cos}})$, and $P(m|z_{\text{cos}})$ is related to $\Phi(M)$ through

$$P(M|z_{\text{cos}}) = \frac{\Phi(M)}{\int_{-\infty}^{M_l(z_{\text{cos}})} \Phi(M) dM}. \quad (2.10)$$

Here $M_l = m_l - 5 \log d_L(z_{\text{cos}})$ is the absolute magnitude which corresponds to the limiting apparent magnitude m_l of the galaxy survey.

Note that the scatter of z_{cos} about the mean relation is not Gaussian. However, the associated 1σ error in the derived angular power spectra depends only on the rms quantity σ_z (see section 2.2 for a detailed discussion of systematic errors). Moreover, the central limit theorem implies that the errors in the power spectra tend to be Gaussian. Considering the actual observations, the two quantities $z_{\text{cos}}(m)$ and $\sigma_z(m)$ can be estimated from the full survey by dividing the data in magnitude bins without actually computing $P(z_{\text{cos}}|m)$. In this case, $\sigma_z(m)$ will include a positive contribution from the cosmological deviations, but this is overwhelmed by both the intrinsic scatter in the $z_{\text{cos}}(m)$ relation and the uncertainties in the photometric redshifts. The underlying assumption is that the sought cosmological deviations between observed and cosmological redshifts cancel out when all galaxies of the entire survey are used. Clearly, a global constant mode should persist in this procedure, but we shall neglect it in this paper, assuming that it does not affect modes in the power spectra on smaller scales. Once we obtain $z_{\text{cos}}(m)$, we compute

$$\Theta_i = \frac{z_i - z_{\text{cos}}(m_i)}{1 + z_i} \quad (2.11)$$

for all galaxies in the survey. Note that in the denominator of the above, we have used z_i instead of $z_{\text{cos}}(m_i)$. This substitution is consistent at linear order and motivated by the fact that z_i is actually a better estimate of the true z_{cos} than $z_{\text{cos}}(m_i)$ which additionally includes deviations from the actual value of z_{cos} due to large random errors with an rms of σ_z .

Environmental dependences of the luminosity distribution on the large-scale density field may systematically shift all Θ_i for galaxies lying in the direction of a certain line of sight. However, we will show below that the resulting signal contamination is small and in any case, it can be removed from the correlations since information on the underlying density field at the relevant scales will be directly available from the observations (see section 2.4).

2.2 Expectations for Euclid

As a test case for a future survey, we consider Euclid which aims at measuring photometric and spectroscopic redshifts of galaxies with $z_{\text{cos}} \sim 1$ over 15,000 deg². More details on the Euclid mission can be found in [9]. Here we focus on the photometric redshift survey since we aim at good statistics rather than precise redshift measurements. Photometric redshifts will be measured with an error of $\sigma_{\text{phot}} \leq 0.05(1 + z_{\text{phot}})$ for ~ 30 galaxies per arcmin², with $z_{\text{cos}} \geq 0.7$ and magnitudes in the broad R+I+Z band (550–920 nm) $\text{RIZ}_{\text{AB}} \leq 24.5$. Estimates of the photometric redshifts will rely on three near-infrared (NIR) bands (Y, J, and H in the range 0.92–2.0 μm) for objects with $\text{Y}_{\text{AB}} \leq 24$, $\text{J}_{\text{AB}} \leq 24$, and $\text{H}_{\text{AB}} \leq 24$. These will further

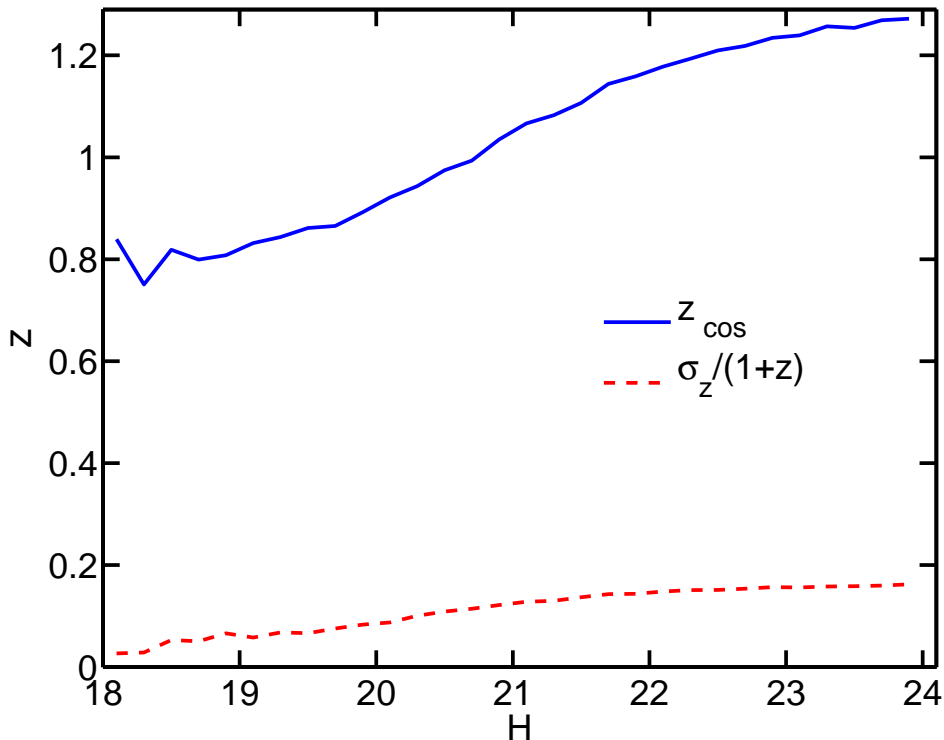


Figure 1. The mean relation $z_{\text{cos}}(m)$ and the corresponding rms scatter $\sigma_z(m)/(1+z)$ for Euclid galaxies with $\text{RIZ}_{\text{AB}} \leq 24.5$, $\text{H}_{\text{AB}} \leq 24$, and photometric redshifts in the range $0.7 < z_{\text{phot}} < 2.0$: The shown results are based on zCOSMOS data.

be complemented by ground-based photometry in the visible bands derived from public data or through engaged collaborations.

The expected number density of Euclid galaxies with measured photometric redshift can be parametrized as follows [11]:

$$n(z_{\text{phot}}) \propto z_{\text{phot}}^2 e^{-(z_{\text{phot}}/z_0)^{3/2}}, \quad (2.12)$$

where $z_0 = z_{\text{mean}}/1.412$ is the peak of the redshift distribution and z_{mean} the median. Here we assume that $z_{\text{mean}} = 0.9$. We have compared the expected distribution $n(z)$ of eq. (2.12) to that measured from galaxies with $\text{H}_{\text{AB}} \leq 24$ and $\text{RIZ}_{\text{AB}} \leq 24.5$ in the zCOSMOS catalog [12–14]. Indeed, we have found that eq. (2.12) does provide a good fit to the data in the range $0.7 < z_{\text{phot}} < 2.0$ which we will consider in our analysis.

The observed $z_{\text{phot}}\text{-H}$ relation of zCOSMOS galaxies has been used to derive $\bar{z}_{\text{phot}}(H)$ and $\sigma_{z_{\text{phot}}}(H)$ in different H-magnitude bins. To match Euclid constraints, we have only considered galaxies with $\text{RIZ}_{\text{AB}} \leq 24.5$, $\text{H}_{\text{AB}} \leq 24$, and $0.7 < z_{\text{phot}} < 2.0$. The additional constraints $\text{Y}_{\text{AB}} \leq 24$ and $\text{J}_{\text{AB}} \leq 24$ do not significantly modify our results and have therefore not been enforced. Our results for the zCOSMOS data are shown in figure 1. The (blue) solid curve and the (red) dashed curve represent the expected $z_{\text{cos}}(H)$ and $\sigma_z(H)$ for Euclid galaxies, respectively. As can be directly read off the figure, the expected scatter in $z_{\text{cos}}(H)$ is $\sigma_z(H) \lesssim 0.3$. Errors on the measured redshift, i.e. σ_{phot} , dominate the scatter for $H < 20$. They will be added in quadrature to determine the effective scatter in the $z_{\text{cos}}\text{-H}$ relation.

Since our aim is to estimate the angular correlation properties of Θ_i , we are concerned with all potential sources of systematic errors that are coherent over large angular scales. Random errors in the H-band photometry and z_{phot} can induce systematic errors as a result of the galaxies' non-uniform distribution in the z_{phot} -H plane. However, the resulting offsets bear no angular coherence and can be safely ignored in our analysis. The lack of angular correlations also characterizes systematic errors induced by a gross misestimate of z_{phot} which are commonly known as “catastrophic errors”.

Angular-dependent systematic errors may arise when calibrating the photometry across a large area of the sky. The angular structure of these errors generally depends on the survey strategy and, considering ground-based observations, its interplay with the atmospheric conditions at the telescope's site. In current surveys such as SDSS, the relative photometric errors are already on the order of 1% (10 mmag) and have only little angular structure [15]. Clearly, these will be further reduced in next-generation surveys, especially in those that will be based in space. Systematic errors of this kind may propagate into zeropoint offsets affecting the estimate of z_{phot} . To assess the significance of this effect for our analysis, we have performed a number of simulations in which we have computed z_{phot} after introducing photometric offsets of about 1% in different bands, using various templates of spectral energy distributions for different galaxy types. As a reference case, we have considered a set of 1000 galaxies at $z = 1$ observed with the Euclid filters RIZ, Y, J, and H. A small, but sizable zeropoint offset $\Delta z_{\text{phot}} = 0.01$ can be obtained if the photometric offset runs smoothly from -5 mmag in RIZ to 5 mmag in the H band. It is rather unlikely that such a configuration will ever occur, but even so, there are plenty of reasons to ignore these systematic errors. First of all, the amplitude and probability of Δz_{phot} decreases dramatically with the number of used filters. For instance, if additional photometry in the visible bands g , r , i , and z is considered (which is expected to be the case for Euclid), then Δz_{phot} drops by a factor of approximately 10. Second, we have found that the offset's amplitude can be further reduced by selecting homogeneous subsamples of objects. Third, Δz_{phot} turns out proportional to the photometry offset, and will decrease when sub-percent calibration accuracy is achieved. Finally, z_{phot} can be independently calibrated in different areas of the sky with the help of spectroscopic redshift information, which may be used to reveal a possible angular correlation among errors.

2.3 Spherical harmonics decomposition for discrete noisy data

Much of the analysis presented below is very similar to previous work done in the lensing community, and before that, in the context of the CMB [16, 17]. As usual, angular power spectra are defined in terms of the spherical harmonics $Y_{lm}(\hat{\mathbf{r}})$. For an all-sky continuous field $f(\hat{\mathbf{r}})$, the decomposition is

$$f_{lm} = \int d\Omega f(\hat{\mathbf{r}}) Y_{lm}(\hat{\mathbf{r}}), \quad f(\hat{\mathbf{r}}) = \sum_{l=0}^{\infty} \sum_{m=-l}^{+l} f_{lm} Y_{lm}^*(\hat{\mathbf{r}}), \quad (2.13)$$

In our case, however, we have to deal with partial sky coverage (around 30% of the sky for Euclid) and consider that the field is sampled at discrete points given by the galaxy positions. The limited sky coverage could formally be described by an appropriate masking of the sphere [18, 19]. However, the description in terms of masks will unnecessarily complicate the notation and somewhat obscure the physical interpretation of the results. We shall therefore resort to a simplified description and assume that we are provided with a survey covering $4\pi f_{\text{sky}}$

steradians of the sky. For each degree l , we assume that there are $(2l + 1)f_{\text{sky}}$ independent modes, instead of $2l + 1$ for full sky coverage. Considering modes with angular resolution much smaller than the extent of the survey, we then have

$$\begin{aligned} \int d\Omega Y_{lm}(\hat{\mathbf{r}}) Y_{l'm'}^*(\hat{\mathbf{r}}) &= f_{\text{sky}} \delta_{ll'}^K \delta_{mm'}^K, \\ \sum_m Y_{lm}(\hat{\mathbf{r}}) Y_{lm}^*(\hat{\mathbf{r}}') &= \frac{(2l + 1)f_{\text{sky}}}{4\pi} P_l(\hat{\mathbf{r}} \cdot \hat{\mathbf{r}}'), \end{aligned} \quad (2.14)$$

where P_l is the Legendre polynomial of degree l . Throughout the paper, the angular integration is carried out only over the observed part of the sky, and the number of terms in the sum of the second relation is $(2l + 1)f_{\text{sky}}$. As is obvious, these relations should be understood to hold in the approximate sense.¹

Considering a function $f(\hat{\mathbf{r}})$ with limited sky coverage in the continuous limit, we define

$$f_{lm} = \frac{1}{f_{\text{sky}}^{1/2}} \int d\Omega f(\hat{\mathbf{r}}) Y_{lm}(\hat{\mathbf{r}}), \quad (2.15)$$

where the integration is again taken over the observed region only. The angular power spectrum C_l is defined as the variance of the f_{lm} 's and given by

$$C_l = \langle |f_{lm}|^2 \rangle_{\text{ens}}, \quad (2.16)$$

where the average is taken over many different realizations of a field with the same power spectrum as f . For brevity, we will use the symbol $\langle \cdot \rangle$ without any subscript to refer to this kind of averaging. Up to cosmic variance, the values of C_l obtained from the ensemble average $\langle |f_{lm}|^2 \rangle$ should equal those computed by averaging over the $(2l + 1)f_{\text{sky}}$ modes for each l . Thus, the angular power spectrum may be estimated as

$$C_l = \langle |f_{lm}|^2 \rangle_m \equiv \frac{1}{(2l + 1)f_{\text{sky}}} \sum_m |f_{lm}|^2. \quad (2.17)$$

In the following, we shall interchange between these different kinds of averaging whenever appropriate. The factor $1/f_{\text{sky}}^{1/2}$ in eq. (2.15) and the rules in eq. (2.14) guarantee that

$$C(\cos \theta) = \sum_l C_l \frac{2l + 1}{4\pi} P_l(\cos \theta), \quad C_l = \int d\Omega C(\cos \theta) P_l(\cos \theta), \quad (2.18)$$

which can be shown by decomposing P_l into Y_{lm} according to the second relation in eq. (2.14) and assuming that $C(\theta)$ is negligible for angular separations larger than the extent of the survey (see appendix A).

For a discrete sampling of f at the positions of N galaxies distributed over the observed part of the sky, we write [20]

$$\sum_i^N f(\hat{\mathbf{r}}_i) \approx \int d\Omega n(\hat{\mathbf{r}}) f(\hat{\mathbf{r}}) \approx \bar{n} \int d\Omega f(\hat{\mathbf{r}}), \quad (2.19)$$

¹We emphasize that a future analysis of the real data should properly account for the lack of a full sky coverage.

where $n(\hat{\mathbf{r}})$ is the projected number density of objects and $\bar{n} = N/(f_{\text{sky}} 4\pi)$ is the corresponding mean number density over the observed part of the sky. Here we have assumed that f itself depends on the density contrast $\delta = n/\bar{n} - 1$, so that the last step applies to linear order in the fluctuations. Again, the angular integration is carried out only over the observed part of the sky. In analogy to eq. (2.15), we further define

$$f_{lm} = \frac{1}{\bar{n} f_{\text{sky}}^{1/2}} \sum_{i=1}^N f(\hat{\mathbf{r}}_i) Y_{lm}(\hat{\mathbf{r}}_i). \quad (2.20)$$

In this case, one can show that the angular power spectrum takes the form (see appendix B)

$$C_l = \langle |f_{lm}|^2 \rangle - \frac{\sigma_f^2}{\bar{n}}, \quad (2.21)$$

where the second term represents the contribution of shot noise due to the discrete sampling of f and $\sigma_f^2 = \sum_i f(\hat{\mathbf{r}}_i)^2/N$. To estimate the values of C_l , we therefore use

$$C_l = \langle |f_{lm}|^2 \rangle_m - \frac{\sigma_f^2}{\bar{n}}. \quad (2.22)$$

If $f_i = S(\hat{\mathbf{r}}_i) + \epsilon_i$ where S is an underlying cosmological signal and ϵ_i is an uncorrelated random error, this simply reflects the fact that $C_l = \langle |S_{lm}|^2 \rangle$. The expected error in this estimate of C_l is given by (again, see appendix B)

$$\Sigma^2 = \frac{2}{(2l+1)f_{\text{sky}}} \left(\frac{\sigma_f^2}{\bar{n}} + C_l \right)^2 \quad (2.23)$$

which includes contributions from both shot noise Σ_{sn} and cosmic variance Σ_{cv} ,

$$\Sigma_{\text{sn}} = \sqrt{\frac{2}{(2l+1)f_{\text{sky}}} \frac{\sigma_f^2}{\bar{n}}}, \quad \Sigma_{\text{cv}} = \sqrt{\frac{2}{(2l+1)f_{\text{sky}}} C_l} \quad (2.24)$$

The variance of the scatter σ_i^2 ,

$$\sigma_i^2 = \langle \epsilon_i^2 \rangle = \frac{\sigma_{\text{phot}}^2(z_i) + \sigma_z^2(m_i)}{(1+z_i)^2}, \quad (2.25)$$

depends on both magnitude and redshift. Note that the factor of $(1+z_i)$ arises from the definition of Θ in eq. (2.1). Considering the application to real data, it is prudent to weight each galaxy according to the σ_i in the sum of eq. (2.20). To minimize the effects of shot noise, we weight each galaxy by a factor of w_i which is given by

$$w_i^2 = \frac{N \sigma_i^{-2}}{\sum_j \sigma_j^{-2}}. \quad (2.26)$$

This particular weighting scheme yields

$$\sigma_f^2 = \frac{N}{\sum_j \sigma_j^{-2}}, \quad (2.27)$$

where we have assumed that the underlying signal makes a negligible contribution to σ_f^2 . The weighting does not affect the ensemble average of $|f_{lm}|^2$, and its net effect is that σ_f should be computed as given by eq. (2.27), i.e. it merely reduces shot noise errors (for additional details, see appendix B). In principle, one may use any weighting scheme.

2.4 Environmental dependences in the luminosity functions and magnification by gravitational lensing

So far, we have assumed that the systematic shifts in the $z_{\text{cos}}(m)$ relation for galaxies in a given direction are solely due to the terms appearing on the right-hand side of eq. (2.1). However, additional shifts may arise from changes in the mean magnitudes due to large-scale density fluctuations in a given direction, i.e. environmental dependences and evolution in the luminosity function, and the magnification effect caused by gravitational lensing. In what follows, we shall denote their contribution as Θ^{env} and Θ^{lens} , respectively. Both effects result in a magnitude shift which translates into additional correlated deviations of the estimated z_{cos} from its mean relation. To model the contribution of these effects in the correlation function of Θ , we need to translate a magnitude shift Δm into a corresponding shift Δz . This can directly be read off the (blue) solid curve $z_{\text{cos}}(m)$ shown in figure 1 in which a shift $\Delta m = 0.2$ leads to mean shift $\Delta z_{\text{cos}} \approx 0.017$.²

To quantify the impact of environmental dependences, we assume that the systematic shift in galaxy magnitude depends on the density contrast δ in regions where they reside, irrespective of the smoothing scale [21, 22]. Here we adopt the linear relation $\Delta m = 0.2\delta$ which is observationally inferred from the visible band [23]. The actual dependence is a function of the photometric band, and it is expected to be much weaker in Euclid’s H-band as indicated by the weak environmental dependence of the Schechter parameter M_* fitted to NIR luminosities [24]. The remaining Schechter parameter, usually dubbed α , exhibits a stronger dependence, but since this parameter fixes the shape at the faint end, it will have only a small impact in deep surveys like Euclid. Nonetheless, it will be possible to remove most of the contamination caused by this effect using the observed distribution of galaxies in the Euclid survey.

In the weak-field limit, the magnification induced by gravitational lensing is proportional to $1 + 2\kappa$, where κ is the effective convergence field, i.e. an integral over the (weighted) density contrast along the line of sight [25]. For a flat Λ CDM model and a fixed source redshift corresponding to a comoving source distance r , one finds

$$\kappa(\boldsymbol{\theta}, r) = \frac{3H_0^2\Omega_0}{2c^2} \int_0^r dr' \frac{r'(r-r')}{a(r')r} \delta(r'\boldsymbol{\theta}, r'), \quad (2.28)$$

where the two-dimensional angular vector $\boldsymbol{\theta}$ is perpendicular to the line of sight. Therefore, it is straightforward to model the magnification and its effect in our analysis. The magnification field contains valuable information since it probes the growth of the angular derivatives of the gravitational potential [e.g. 25, 26]. It can also be used to constrain the gravitational slip which arises in certain modifications of the general theory of relativity [e.g. 27, 28]. Given a theory of gravity, much of the contribution to the power spectra from gravitational lensing can, in principle, be removed using the underlying large-scale density field which is inferred from the foreground galaxy distribution. Considering the following analysis, however, we will treat the effects of lensing magnification as part of the signal. As we will see below, its contribution is not negligible, and can be constrained together with the power spectrum of the velocity field.

²Note that although more complicated schemes are possible, we adopt this mean relation for simplicity.

3 Theoretical angular power spectra

In the following, we will present predictions for the angular power spectra corresponding to the various terms in eq. (2.1). Since the observed galaxies cover a redshift range $z_1 < z < z_2$, we do not consider the angular power spectra of a quantity f defined at a specific redshift, but instead we use

$$\tilde{f}(\hat{\mathbf{r}}) = \int_{r_1}^{r_2} f[\hat{\mathbf{r}}r, t(r)] p(r) dr, \quad (3.1)$$

where r_1 and r_2 are the comoving distances at the survey's limiting redshifts, z_1 and z_2 , respectively, and $p(r)dr$ is the probability of observing a galaxy within the interval $[r, r + dr]$. Note that the function f represents any of the terms on the right-hand side of eq. (2.1), i.e. Θ^V , Θ^Φ , and $\Theta^{\dot{\Phi}}$. Beginning with Θ^Φ , we write

$$\tilde{\Theta}^\Phi_{lm} = \int d\Omega \tilde{\Theta}^\Phi Y_{lm}(\hat{\mathbf{r}}) = \frac{1}{c^2} \int d\Omega Y_{lm}(\hat{\mathbf{r}}) \int_{r_1}^{r_2} W_\phi(r) \Phi_0(\hat{\mathbf{r}}r) dr, \quad (3.2)$$

where we have used the linear relation $\Phi(\mathbf{r}, t) = (D/a)\Phi_0(\mathbf{r}, t_0)$ and defined $W_\phi = Dp(r)/a$, with $D(t)$ and $a(t)$ evaluated at $t = t(r)$. Expanding $\Phi_0(\mathbf{r})$ in Fourier space,

$$\Phi_0(\mathbf{r}) = \frac{1}{(2\pi)^3} \int d^3k \Phi_{\mathbf{k}} e^{i\mathbf{k}\cdot\mathbf{r}}, \quad (3.3)$$

and using

$$e^{i\mathbf{k}\cdot\mathbf{r}} = 4\pi \sum_{l,m} i^l j_l(kr) Y_{lm}^*(\hat{\mathbf{n}}) Y_{lm}(\hat{\mathbf{k}}), \quad (3.4)$$

where j_l is the usual first-kind spherical Bessel function of degree l , we get

$$\tilde{\Theta}^\Phi_{lm} = \frac{i^l}{2\pi^2 c^2} \int_{r_1}^{r_2} dr W_\phi \int d^3k \Phi_{\mathbf{k}} j_l(kr) Y_{lm}(\hat{\mathbf{k}}). \quad (3.5)$$

Therefore, we finally arrive at

$$C_l^\Phi = \langle |\tilde{\Theta}^\Phi_{lm}|^2 \rangle = \frac{2}{\pi c^4} \int dk k^2 P_\Phi(k) \left| \int_{r_1}^{r_2} dr W_\phi j_l(kr) \right|^2, \quad (3.6)$$

where we have used $\langle \Phi_{\mathbf{k}} \Phi_{\mathbf{k}'} \rangle = (2\pi)^3 \delta^D(\mathbf{k} - \mathbf{k}') P_\Phi(k)$. Similarly, using the linear relation in eq. (2.4), we obtain

$$C_l^V = \frac{2}{\pi c^2} \int dk k^2 P_\Phi(k) \left| \int_{r_1}^{r_2} dr W_V \left(\frac{l j_l}{r} - k j_{l+1} \right) \right|^2, \quad (3.7)$$

where $W_V = 2a\dot{D}p(r)/3\Omega_0 H_0^2$. As for $\Theta^{\dot{\Phi}}$, the last term appearing in eq. (2.1), we will assume that the signal is mostly caused by the large-scale structure between the observed high redshift galaxy sample and the observer. Therefore, $\Theta^{\dot{\Phi}}$ is approximately the same for all galaxies along a common line-of-sight such that $\tilde{\Theta}^{\dot{\Phi}} \approx \Theta^{\dot{\Phi}}$. The angular power spectrum then reads

$$C_l^{\dot{\Phi}} = \langle |\Theta^{\dot{\Phi}}_{lm}|^2 \rangle = \frac{8}{\pi c^6} \int dk k^2 P_\Phi(k) \left| \int_0^r dr' W_{\dot{\Phi}} j_l(kr') \right|^2, \quad (3.8)$$

where $W_{\dot{\Phi}}(t)/a = (d/dt)[D/a]$. The integration over r' is taken from $r = 0$ out to a distance beyond which Φ becomes nearly constant with time. For simplicity, we will assume that

most of the contribution to the integral comes from the inner edge of the considered galaxy sample, and adopt $z = 1$ in eq. (3.8) for all galaxies in the survey. For Euclid, this seems to be the case since the mean redshift is expected to be $z \sim 1$. Note that the same assumptions are used when calculating the angular power spectrum C^{lens} . Although not explicitly given, similar expressions may be obtained for the corresponding cross-correlations of the above contributions.

3.1 Predictions of the Λ CDM scenario

Having derived the relevant expressions above, we are now ready to make predictions for the framework of Λ CDM. Here we adopt a spatially flat model with best-fit parameters based on the CMB anisotropies measured by the Wilkinson Microwave Anisotropy Probe (WMAP) [29]. In this case, the total mass density parameter is $\Omega_m = 0.266$, the baryonic density parameter $\Omega_b = 0.0449$, the Hubble constant $h = 0.71$ in units of $100 \text{ km s}^{-1} \text{ Mpc}^{-1}$, the scalar spectral index $n_s = 0.963$, and $\sigma_8 = 0.80$ for the rms of linear density fluctuations within spheres of $8h^{-1} \text{ Mpc}$. We work with a parametric form of the power spectrum taken from ref. [30] (see eqs. 29–31 in their paper). For the calculation of angular power spectra, we use the expressions from section 3 together with $p(r)$ corresponding to the redshift distribution of galaxies appropriate for Euclid which is given by eq. (2.12).

The angular power spectra and associated errors are plotted in figure 2. The shot-noise error Σ_{sn} is computed using eqs. (2.25) and (2.27), which gives $\sigma_f = 0.17$ as inferred from the (red) dashed curve in figure 1. For completeness, we also show the power spectrum C^{env} which results from environmental dependences in the luminosity function. As explained in section 2.4, the contamination arising from this effect can be removed given the observed distribution of galaxies in the survey. The accuracy to which this can be achieved for Euclid is represented by Σ_{env} , the 1σ error within which C^{env} can be estimated explicitly from the data (see appendix B for details). As is clear from C^{lens} in the figure, magnification caused by gravitational lensing introduces significant angular correlations in $(z_i - z_{\text{cos}})/(1 + z_i)$.

The quantity C^{tot} is the power spectrum of the sum of the three signals Θ^{lens} , Θ^{V} , and Θ^{Φ} , corresponding to the lensing magnification, the Doppler shift, and the gravitational shift, respectively. Note that the calculation of C^{tot} does include covariance between the three individual signals. The contribution from Θ^{Φ} is negligible as is indicated by C^{Φ} , and we do not include it in C^{tot} . At $l \lesssim 10$, C^{V} is the dominant contribution, but the lensing term C^{lens} takes over at $l \gtrsim 10$ –15, roughly until $l \sim 60$ where it drops below the shot-noise level. The shaded area represents the 1σ error of C^{tot} due to cosmic variance. For practical purposes, it is therefore possible to provide measurements of C^{V} and C^{lens} by an appropriate fitting procedure of the two corresponding curves to the measured C^{tot} . Unfortunately, at low l , cosmic variance is so large that accurate constraints on C^{Φ} do not seem possible.

3.2 Signal-to-noise and expected error on model normalization

Suppose that observations yield an estimate C_l^{obs} for the total power spectrum C_l^{tot} . Let $C_l^{\text{H}_0} = 0$ and $C_l^{\text{H}_1}$ be the expected total power spectra for the null hypothesis with no correlations (H_0) and of the Λ CDM model (H_1), respectively. The ratio of probabilities for H_1 and H_0 is given by

$$-2 \ln \frac{P(H_0)}{P(H_1)} = \sum_l \left[\frac{(C_l^{\text{obs}} - C_l^{\text{H}_0})^2}{\Sigma_{\text{sn}}^2} - \frac{(C_l^{\text{obs}} - C_l^{\text{H}_1})^2}{\Sigma^2} + 2 \ln \left(\frac{\Sigma_{\text{sn}}}{\Sigma} \right) \right]. \quad (3.9)$$

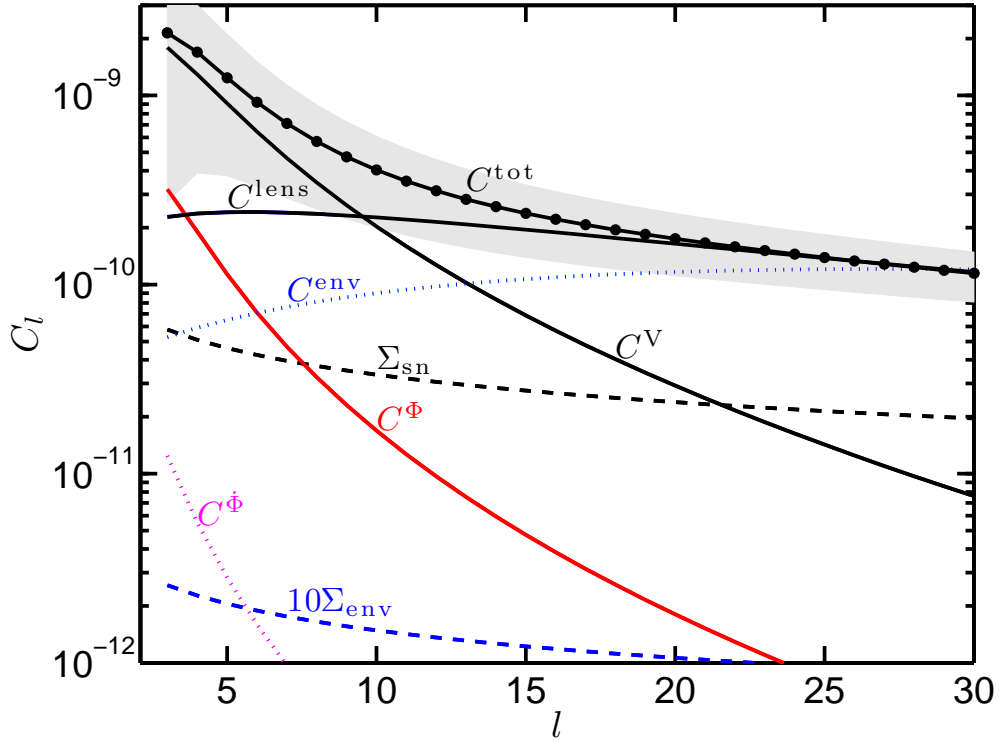


Figure 2. Angular power spectra in the Λ CDM model as explained in the text: The shaded area represents the cosmic variance uncertainty Σ_{cv} on C_l^{tot} , and Σ_{sn} is the 1σ shot-noise error for the Euclid survey. The desired signal is contaminated by C_l^{env} which results from environmental dependences in the luminosity function and can be removed from the actual Euclid data with high precision represented by Σ_{env} . Only contributions (including cross-correlations) from Θ^{V} (peculiar velocity), Θ^{Φ} (gravitational shift), and Θ^{lens} (lensing magnification) are included in C_l^{tot} . At $l \sim 60$ (not shown), Σ_{sn} and C_l^{tot} become comparable.

If H_1 holds, it follows that $C_l^{\text{H}_1}$ is equal to the C_l^{tot} shown in figure 2, and $C_l^{\text{obs}} - C_l^{\text{H}_1}$ is a random variable with variance Σ^2 given by eq. (2.23). Therefore, the signal-to-noise ratio (S/N) for rejecting H_0 is

$$\left(\frac{S}{N}\bigg|_0\right)^2 = -2\ln\frac{P(H_0)}{P(H_1)} = \sum_l \left[\frac{(2l+1)f_{\text{sky}}C_l^2}{2\sigma_f^4/\bar{n}^2} + \left(1 + \frac{\bar{n}C_l}{\sigma_f^2}\right)^2 - 2\ln\left(1 + \frac{\bar{n}C_l}{\sigma_f^2}\right) \right], \quad (3.10)$$

where $C_l = C_l^{\text{H}_1} = C_l^{\text{tot}}$. Substituting the relevant quantities into the above, we obtain $(S/N)|_0 = 101$, where the above sum rapidly converges by $l = 30$. On the other hand, if H_0 is true, then the S/N for rejecting H_1 is given by

$$\begin{aligned} \left(\frac{S}{N}\bigg|_1\right)^2 &= -2\ln\frac{P(H_1)}{P(H_0)} \\ &= \sum_l \left[\frac{(2l+1)f_{\text{sky}}C_l^2}{2(\sigma_f^2/\bar{n} + C_l)^2} + \left(1 + \frac{\bar{n}C_l}{\sigma_f^2}\right)^{-2} + 2\ln\left(1 + \frac{\bar{n}C_l}{\sigma_f^2}\right) \right], \end{aligned} \quad (3.11)$$

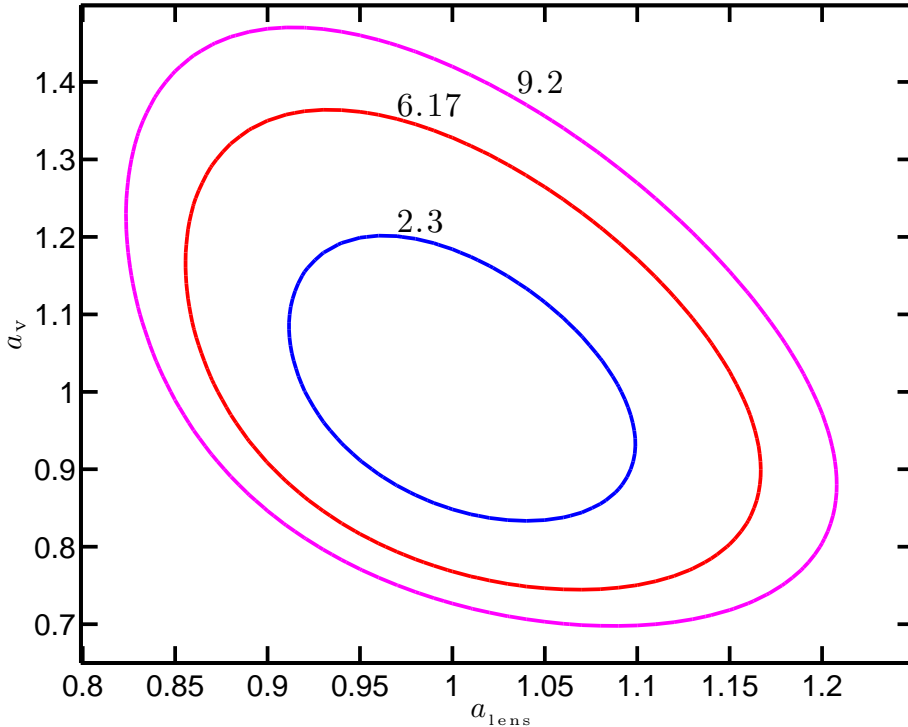


Figure 3. Confidence levels for measuring the amplitudes of the velocity and lensing power spectra by fitting $a_v^2 C^V + a_{\text{lens}}^2 C^{\text{lens}}$ to random realizations of C^{tot} which include both shot noise and cosmic variance: The fitting procedure ignores physical cross-correlations between the used quantities. Contours are shown for $\Delta\chi^2 = 2.3, 6.17,$ and 9.2 , corresponding to confidence levels of 68%, 95.4% and 99%, respectively.

which quickly converges at $l \sim 50$ and yields $(S/N)|_1 = 14.7$. The fact that $(S/N)|_1 \ll (S/N)|_0$ is a result of cosmic variance which is zero for the H_0 hypothesis, but significant in the Λ CDM scenario, i.e. $\Sigma_{\text{cv}}^2 = 2C_l^2/(2l+1)f_{\text{sky}}$.

In addition to S/N considerations, we can assess how well a measurement of C^{tot} would constrain the normalization of the Λ CDM power spectrum in terms of σ_8 . To this end, we write the model's total power spectrum as $C^{\text{tot,m}} = (\sigma_8/0.8)^2 C^{\text{tot}}$, where C^{tot} as illustrated in figure 2 is obtained for $\sigma_8 = 0.8$. The expected 1σ error on σ_8 is then $(-\partial^2 \ln P(H_1)/\partial \sigma_8^2)^{-1}$, where $P(H_1)$ is now expressed as

$$\ln P(H_1) = - \sum_l \frac{(C_l^{\text{obs}} - C_l^{\text{tot,m}})^2}{2\Sigma_l^2} - \sum_l \ln \Sigma_l, \quad (3.12)$$

and Σ_l is given by eq. (2.23) with $C_l = C_l^{\text{tot,m}}$. Using a normal probability distribution of the form given in eq. (3.12) with fixed $\sigma_8 = 0.8$, we have generated 1000 random realizations of C^{obs} . For each of these realizations, we have maximized $P(H_1)$ given by eq. (3.12) with respect to σ_8 . As a result, we find that the true value $\sigma_8 = 0.8$ is recovered within a relative 1σ error of less than 4%, without any statistically significant bias.

We have also inspected the possibility of constraining the velocity and lensing signal amplitudes with the help of the two-parameter model

$$C^{\text{tot,m}} = a_v^2 C^V + a_{\text{lens}}^2 C^{\text{lens}}. \quad (3.13)$$

This model for $C^{\text{tot,m}}$ neglects the contribution of Θ^Φ to C^{obs} as well as any covariance between the remaining signals, Θ^V and lensing magnification Θ^{lens} . Using the above expression, we have repeated the procedure described above for constraining σ_8 with the 1000 random realizations of C^{obs} . The result is presented in figure 3 which shows contours of $\Delta\chi^2 = -2\ln P + 2\ln \max(P)$ as a function of a_V and a_{lens} . The contours have been computed for one of the random realizations, but the values of the best-fit parameters (giving the lowest $\Delta\chi^2$) obtained for this particular realization have been shifted to their underlying value, i.e. unity for both. This is reasonable since the average best-fit parameters of 1000 realizations are essentially unbiased. As seen from the figure, a_{lens} is constrained with better accuracy than the velocity amplitude a_V . This is consistent with figure 1 which shows that C^{lens} dominates the total signal over a large range of l while C^V is significant only for low l where cosmic variance becomes increasingly important. Still, both parameters are constrained with good accuracy.

4 Discussion

In this paper, we have presented a novel method for deriving direct constraints on the peculiar velocity and gravitational potential power spectra from currently planned galaxy redshift surveys. The large number of galaxies with photometric redshifts in these surveys allows one to exploit apparent galaxy magnitudes as a proxy for their cosmological redshifts since it beats down the large scatter in the $z_{\text{cos}}(m)$ relation and the uncertainty in the photometric redshifts. The method aims at directly constraining power spectra of the underlying fluctuation fields independent of the way galaxies trace mass. Other methods for extracting cosmological information from redshift surveys rely on accurate measurements of the galaxy power spectrum in redshift space (since galaxy distances remain unknown). The power spectrum and other statistical measures based on the distribution of galaxies have been successful at probing the nature of dark matter and placing important constraints on neutrino masses [31–33]. Having said that, however, they depend on a very accurate knowledge of the relation between galaxies and the full underlying matter distribution. The method we have considered here is less precise, but it is completely independent of the galaxy formation process and offers a much more sensitive assessment of the underlying physical mechanism driving cosmic acceleration and structure formation. This approach is particularly worthwhile if such constraints on the velocity field and the gravitational potential are contrasted with local constraints obtained from data at low redshifts. For example, peculiar motions of galaxies within a distance of $\sim 100h^{-1}$ Mpc can be measured using tight relations between intrinsic observables of galaxies [e.g. 34, 35], and also using astrometric observations of the Gaia space mission which is currently scheduled for launch in 2013. These peculiar motions of galaxies have been useful for constraining cosmological parameters [36] as well as the amplitude of the velocity field in the nearby Universe [5, 37].

Although we have presented predictions for the Euclid survey, the science proposed in this paper will not have to wait for this space mission. In fact, several ground-based photometric surveys in the optical and near-infrared bands, which will constitute the backbone of Euclid’s photometry, will provide photometric redshift catalogs that can be used for our purposes well before the launch of the satellite. On a shorter timescale, the VLT Survey Telescope (VST) will be used to carry out the Kilo Degree Survey (KiDS), one of the ESO public surveys. It will cover $1,500 \text{ deg}^2$ to $u = 24$, $g = 24.6$, $r = 24.4$, and $i = 23.1$, and will

probably contain $\sim 10^8$ galaxies with measured photometric redshifts.³ Also, the Dark Energy Survey (DES) will start its operations soon, and it will cover 5000 deg² of the Southern sky within 5 years, reaching magnitudes up to ~ 24 in SDSS *griz* filters, comparable to the limiting magnitudes of Euclid and with a redshift distribution dN/dz similar to that of Euclid galaxies. DES will measure photometric redshifts of $\sim 3 \times 10^8$ galaxies with $\sigma_{\text{photo}} \sim 0.12$ at $z \sim 1$.⁴ Furthermore, the first of the four planned Pan-STARRS telescopes has been operational since May 2010.⁵ The planned 3π area of the sky will be considerably shallower, detecting galaxies below a limiting magnitude of ~ 24 in the *griz* bands. A deeper survey involving the PS1 and PS2 telescopes is currently being planned. The survey should cover $\sim 7,500\text{deg}^2$ with limiting fluxes $g = 24.7$, $r = 24.3$, $i = 24.1$, and $z = 23.6$. Photometric redshifts will then be measured for $\sim 4.5 \times 10^8$ galaxies with similar errors. Finally, on the long run, the Large Synoptic Survey Telescope (LSST) is expected to start operations in 2020. Its main deep-wide-fast survey is expected to observe $\sim 20,000 \text{ deg}^2$ in the *ugrizy* bands. After about 10 years of operation, it will reach much deeper depths (down to a co-added magnitude $r = 27$), detecting about 3×10^9 galaxies [38].

Acknowledgments

We are grateful to Micol Bolzonella for computing all redshift-magnitude relations used in this paper from the zCOSMOS data and for running simulations to assess the amplitude of zeropoint errors on the measured photometric redshifts. We also thank Henry McCracken for providing us with the H-band magnitudes of zCOSMOS galaxies. E.B. thanks Gianni Zamorani and Massimo Meneghetti for useful discussions and suggestions. This work was supported by THE ISRAEL SCIENCE FOUNDATION (grant No.203/09), the German-Israeli Foundation for Research and Development, the Asher Space Research Institute and the WINNIPEG RESEARCH FUND. E.B. acknowledges the support provided by MIUR PRIN 2008 “Dark energy and cosmology with large galaxy surveys” and by Agenzia Spaziale Italiana (ASI-Uni Bologna-Astronomy Dept. ‘Euclid-NIS’ I/039/10/0). M.F. is supported in part at the Technion by the Lady Davis Foundation.

A Proof of the relations in eq. (2.18)

For any function $f(\hat{\mathbf{r}})$, we have defined

$$f_{lm} = \frac{1}{f_{\text{sky}}^{1/2}} \int d\Omega f(\hat{\mathbf{r}}) Y_{lm}(\hat{\mathbf{r}}) . \quad (\text{A.1})$$

³<http://www.eso.org/public/teles-instr/surveytelescopes/vst.html>

⁴<http://www.darkenergysurvey.org/reports/proposal-standalone.ps>

⁵<http://pan-starrs.ifa.hawaii.edu/public/home.html>

Using the relations given in eq. (2.14), we get

$$\begin{aligned}
C_l &= \frac{1}{(2l+1)f_{\text{sky}}} \sum_m \langle |f_{lm}|^2 \rangle \\
&= \frac{1}{(2l+1)f_{\text{sky}}^2} \int d\Omega d\Omega' \langle f(\hat{\mathbf{r}}) f(\hat{\mathbf{r}}') \rangle \sum_m Y_{lm}(\hat{\mathbf{r}}) Y_{lm}^*(\hat{\mathbf{r}}') \\
&= \frac{1}{4\pi f_{\text{sky}}} \int d\Omega d\Omega' C(\hat{\mathbf{r}} \cdot \hat{\mathbf{r}}') P_l(\hat{\mathbf{r}} \cdot \hat{\mathbf{r}}') \\
&= \frac{1}{4\pi f_{\text{sky}}} \int d\Omega' \int d\Omega C(\hat{\mathbf{r}} \cdot \hat{\mathbf{r}}') P_l(\hat{\mathbf{r}} \cdot \hat{\mathbf{r}}') \\
&= \int d\Omega C(\cos \theta) P_l(\cos \theta),
\end{aligned} \tag{A.2}$$

where for the last step, we have used that the integral over $d\Omega$ is independent of $\hat{\mathbf{r}}'$, assuming that the coherence angular length is smaller than the spatial extent of the survey. Similarly, the first relation in eq. (2.18) follows from substituting it into the second and exploiting the (near) orthogonality of $P_l(\cos \theta)$.

B Estimating angular power spectra for discrete data

Just as in the main body of the paper, we will take the symbol $\langle (\cdot) \rangle_m \equiv (1/(2l+1)f_{\text{sky}}) \sum_m (\cdot)$ to denote averaging over all indices m corresponding to the degree l of the spherical harmonic decomposition. Again, the symbol $\langle \cdot \rangle$ without any subscript will refer to the previously introduced ensemble average, and we shall interchange between $\langle \cdot \rangle_m$ and $\langle \cdot \rangle$ whenever appropriate. For brevity of notation, we also use the definition $Y_m^i \equiv Y_{lm}(\hat{\mathbf{r}}_i)$, thus omitting the subscript l since all calculations will refer to a given degree l of the spherical harmonics. Starting from the definition of f_{lm} in eq. (2.20), we obtain

$$\begin{aligned}
\langle |f_{lm}|^2 \rangle &= \frac{1}{\bar{n}^2 f_{\text{sky}}} \sum_{i,j} \langle f_i f_j \rangle Y_m^i Y_m^{*j} \\
&= \frac{1}{\bar{n}^2 f_{\text{sky}}} \sum_i \langle f_i^2 \rangle |Y_m^i|^2 + \frac{1}{\bar{n}^2 f_{\text{sky}}} \sum_{i \neq j} \langle f_i f_j \rangle Y_m^i Y_m^{*j} \\
&= \frac{\sigma_f^2}{\bar{n}} + C_l,
\end{aligned} \tag{B.1}$$

where the value of σ_f is inferred from the $z_{\cos}(m)$ relation, i.e. $\sigma_f^2 = \sum_i \sigma_i^2 / N$. As our estimate for C_l , we therefore take

$$C_l = \langle |f_{lm}|^2 \rangle_m - \frac{\sigma_f^2}{\bar{n}}. \tag{B.2}$$

Another way of arriving at this result is to partition the observed sky into infinitesimally small cells of angular size $\delta\Omega$, with each cell containing at most one galaxy [19]. In this case, we write

$$f_{lm} = \frac{1}{\bar{n} f_{\text{sky}}^{1/2}} \sum_{\alpha} f_{\alpha} n_{\alpha} Y_m^{\alpha}, \tag{B.3}$$

where n_α , the number of galaxies in cell α , is either 0 or 1. Using that $\langle n_\alpha \rangle = \bar{n}\delta\Omega$ in this representation, we obtain the expression

$$\begin{aligned}
\langle |f_{lm}|^2 \rangle &= \frac{1}{\bar{n}^2 f_{\text{sky}}} \sum_{\alpha, \beta} \langle f_\alpha f_\beta \rangle \langle n_\alpha n_\beta \rangle Y_m^\alpha Y_m^{*\beta} \\
&= \frac{1}{\bar{n}^2 f_{\text{sky}}} \sum_{\alpha} \langle f_\alpha^2 \rangle \langle n_\alpha^2 \rangle |Y_m^\alpha|^2 + C_l \\
&= \frac{1}{\bar{n}^2 f_{\text{sky}}} \sum_{\alpha} \langle f_\alpha^2 \rangle \bar{n} \delta\Omega |Y_m^\alpha|^2 + C_l \\
&= \frac{\sigma_f^2}{\bar{n}} + C_l,
\end{aligned} \tag{B.4}$$

where we have used the relation $n_\alpha^2 = n_\alpha$. We find this particular approach a little more intuitive to compute the expected error of the estimate in eq. (B.2). Let f^r and n^r be possible random realizations of the data in another universe. The variance of the error in C_l may then be written as an ensemble average over these realizations, i.e.

$$\begin{aligned}
\Sigma^2 &= \langle (C_l^r - C_l)^2 \rangle \\
&= \left\langle \left(\frac{1}{\bar{n}^2 f_{\text{sky}}} \sum_{\alpha \neq \beta} f_\alpha^r f_\beta^r n_\alpha^r n_\beta^r \langle Y_m^\alpha Y_m^{*\beta} \rangle_m - C_l \right)^2 \right\rangle \\
&= \frac{1}{\bar{n}^4 f_{\text{sky}}^2} \sum_{\alpha \neq \beta, \alpha' \neq \beta'} \langle f_\alpha^r n_\alpha^r f_\beta^r n_\beta^r f_{\alpha'}^r n_{\alpha'}^r f_{\beta'}^r n_{\beta'}^r \rangle \langle Y_m^\alpha Y_m^{*\beta} \rangle_m \langle Y_m^{\alpha'} Y_m^{*\beta'} \rangle_{m'} - C_l^2.
\end{aligned} \tag{B.5}$$

Note the remarkable fact that due to the uncorrelated nature of the errors and because $\alpha \neq \beta$ as well as $\alpha' \neq \beta'$, only second-order moments of n and f contribute to Σ^2 . This is important since it implies that the non-Gaussian nature of the scatter in the $z_{\text{cos}}(m)$ relation does not affect the variance of errors in the estimated C_l . Assuming that fn is a Gaussian random field, we further have

$$\begin{aligned}
\langle f_\alpha^r n_\alpha^r f_\beta^r n_\beta^r f_{\alpha'}^r n_{\alpha'}^r f_{\beta'}^r n_{\beta'}^r \rangle &= \langle f_\alpha^r f_\beta^r n_\alpha^r n_\beta^r \rangle \langle f_{\alpha'}^r f_{\beta'}^r n_{\alpha'}^r n_{\beta'}^r \rangle \\
&\quad + \langle f_\alpha^r f_{\alpha'}^r n_\alpha^r n_{\alpha'}^r \rangle \langle f_\beta^r f_{\beta'}^r n_\beta^r n_{\beta'}^r \rangle \\
&\quad + \langle f_\alpha^r f_{\beta'}^r n_\alpha^r n_{\beta'}^r \rangle \langle f_{\alpha'}^r f_\beta^r n_{\alpha'}^r n_\beta^r \rangle.
\end{aligned} \tag{B.6}$$

Considering the above, averages with no equal indices will contribute terms proportional to C_l^2 in the sum of eq. (B.5). Neglecting the contribution of shot noise, this would yield the usual cosmic variance expression $2C_l^2/(2l+1)f_{\text{sky}}$. For the case $\alpha = \alpha'$ and $\beta = \beta'$, the second term on the right-hand side of eq. (B.6) turns into $\sigma_f^4(\bar{n}\delta\Omega)^2$, where we have again used that $\langle n_\alpha^2 \rangle = \langle n_\alpha \rangle = \bar{n}\delta\Omega$. The other combination which makes the same contribution is $\alpha = \beta'$ and $\alpha' = \beta$. A bit of algebra shows that the contribution to the variance in eq. (B.5) of these two combinations is $2\sigma_f^4/(2l+1)\bar{n}^2 f_{\text{sky}}$. For $\alpha = \alpha'$ and $\beta \neq \beta'$, the second term on the right-hand side of eq. (B.6) simplifies to $\sigma_f^2 \langle f_\beta^r f_{\beta'}^r \rangle (\bar{n}\delta\Omega)^3$, and the total result of similar permutations with only two equal indices reads $4\sigma_f^2 C_l/(2l+1)\bar{n} f_{\text{sky}}$. Finally, summing up all relevant terms leads to

$$\Sigma^2 = \frac{2}{(2l+1)f_{\text{sky}}} \left(\frac{\sigma_f^2}{\bar{n}} + C_l \right)^2. \tag{B.7}$$

Using the weights defined in eq. (2.26), it is easy to say that the same results are valid with σ_f given by eq. (2.27).

In the main body of the paper, we have assumed that environmental dependences of the galaxy luminosity function arise due to variations in the large-scale density contrast. The signal contamination associated with this effect has an angular power spectrum which is proportional to that of the density contrast. In the following, we give an estimate for this power spectrum and the 1σ error within which it can be constrained from the observed galaxy distribution. To begin with, we consider [19]

$$\delta_{lm} = \frac{1}{\bar{n}f_{\text{sky}}^{1/2}} \sum_{\alpha} n_{\alpha} Y_m^{\alpha}. \quad (\text{B.8})$$

For the f_{lm} 's, we have assumed that n_{α} is a discrete sampling of a uniform distribution. That was consistent with linear theory since we have assumed that f is a function of the density contrast. However, now we are interested in the autocorrelation function of n_{α} , and thus the treatment of δ_{lm} is a little different. To obtain an estimate for the angular power spectrum of the density contrast, we write

$$\begin{aligned} \langle |\delta_{lm}|^2 \rangle &= \frac{1}{\bar{n}^2 f_{\text{sky}}} \sum_{\alpha, \beta} \langle n_{\alpha} n_{\beta} \rangle Y_m^{\alpha} Y_m^{\beta} \\ &= \frac{1}{\bar{n}} + C_l^{\delta\delta}. \end{aligned} \quad (\text{B.9})$$

Similar as before, we hence take $C_l^{\delta\delta} = \langle |\delta_{lm}|^2 \rangle_m - 1/\bar{n}$ as our estimate of the angular power spectrum of δ . The statistical error in this estimate can be derived using the same approach as above, and it is given by

$$\Sigma_{\delta\delta}^2 = \frac{2}{(2l+1)f_{\text{sky}}} \left(\frac{1}{\bar{n}} + C_l^{\delta\delta} \right)^2. \quad (\text{B.10})$$

One of the main interests in this paper is to remove the contamination C_l^{env} to the signal C_l^{tot} using the actually observed distribution of galaxies. Note that in this case, cosmic variance is irrelevant to the analysis since we are referring to a given data set rather than the expected deviation of the estimated power spectrum from some underlying theoretical model. Therefore, we may simply neglect the contribution of cosmic variance in eq. (B.10), and the variance of the relevant error reduces to the expression $2/(2l+1)\bar{n}f_{\text{sky}}$.

References

- [1] D. Lynden-Bell, S. M. Faber, D. Burstein, R. L. Davies, A. Dressler, R. J. Terlevich, and G. Wegner, *Spectroscopy and photometry of elliptical galaxies. V - Galaxy streaming toward the new supergalactic center*, *ApJ* **326** (Mar., 1988) 19–49.
- [2] M. A. C. Perryman, K. S. de Boer, G. Gilmore, E. Høg, M. G. Lattanzi, L. Lindegren, X. Luri, F. Mignard, O. Pace, and P. T. de Zeeuw, *GAIA: Composition, formation and evolution of the Galaxy*, *A&A* **369** (Apr., 2001) 339–363, [[astro-ph/0101235](#)].
- [3] A. Nusser, E. Branchini, and M. Davis, *Gaia: a Window to Large Scale Flows*, *ArXiv e-prints* (Feb., 2012) [[arXiv:1202.4138](#)].
- [4] A. Nusser, E. Branchini, and M. Davis, *Bulk Flows from Galaxy Luminosities: Application to 2Mass Redshift Survey and Forecast for Next-generation Data Sets*, *ApJ* **735** (July, 2011) 77, [[arXiv:1102.4189](#)].

- [5] A. Nusser and M. Davis, *The Cosmological Bulk Flow: Consistency with Λ CDM and $z \approx 0$ Constraints on σ_8 and γ* , *ApJ* **736** (Aug., 2011) 93, [[arXiv:1101.1650](#)].
- [6] E. Branchini, M. Davis, and A. Nusser, *The linear velocity field of 2MASS Redshift Survey, $K_s = 11.75$ galaxies: constraints on β and bulk flow from the luminosity function*, *MNRAS* (May, 2012) 3161, [[arXiv:1202.5206](#)].
- [7] G. A. Tammann, A. Yahil, and A. Sandage, *The velocity field of bright nearby galaxies. II - Luminosity functions for various Hubble types and luminosity classes - The peculiar motion of the local group relative to the Virgo cluster*, *ApJ* **234** (Dec., 1979) 775–784.
- [8] R. Laureijs, *Euclid Assessment Study Report for the ESA Cosmic Visions*, *ArXiv e-prints* (Dec., 2009) [[arXiv:0912.0914](#)].
- [9] R. Laureijs, J. Amiaux, S. Arduini, J. . Auguères, J. Brinchmann, R. Cole, M. Cropper, C. Dabin, L. Duvet, A. Ealet, and et al., *Euclid Definition Study Report*, *ArXiv e-prints* (Oct., 2011) [[arXiv:1110.3193](#)].
- [10] R. K. Sachs and A. M. Wolfe, *Perturbations of a Cosmological Model and Angular Variations of the Microwave Background*, *ApJ* **147** (Jan., 1967) 73.
- [11] L. Amendola, S. Appleby, D. Bacon, T. Baker, M. Baldi, N. Bartolo, A. Blanchard, C. Bonvin, S. Borgani, E. Branchini, et al., *Cosmology and fundamental physics with the Euclid satellite*, *ArXiv e-prints* (June, 2012) [[arXiv:1206.1225](#)].
- [12] O. Ilbert, P. Capak, M. Salvato, H. Aussel, H. J. McCracken, D. B. Sanders, N. Scoville, J. Kartaltepe, S. Arnouts, E. Le Floch, et al., *Cosmos Photometric Redshifts with 30-Bands for 2-deg²*, *ApJ* **690** (Jan., 2009) 1236–1249, [[arXiv:0809.2101](#)].
- [13] H. J. McCracken, P. Capak, M. Salvato, H. Aussel, D. Thompson, E. Daddi, D. B. Sanders, J.-P. Kneib, C. J. Willott, C. Mancini, et al., *The COSMOS-WIRCam Near-Infrared Imaging Survey. I. BzK-Selected Passive and Star-Forming Galaxy Candidates at $z_{\text{gsim}} 1.4$* , *ApJ* **708** (Jan., 2010) 202–217, [[arXiv:0910.2705](#)].
- [14] R. Bielby, P. Hudelot, H. J. McCracken, O. Ilbert, E. Daddi, O. Le Fèvre, V. Gonzalez-Perez, J.-P. Kneib, C. Marmo, Y. Mellier, M. Salvato, D. B. Sanders, and C. J. Willott, *The WIRCam Deep Survey I: Counts, colours and mass-functions derived from near-infrared imaging in the CFHTLS Deep Fields*, *ArXiv e-prints* (Nov., 2011) [[arXiv:1111.6997](#)].
- [15] N. Padmanabhan, D. J. Schlegel, D. P. Finkbeiner, J. C. Barentine, M. R. Blanton, H. J. Brewington, J. E. Gunn, M. Harvanek, D. W. Hogg, Ž. Ivezić, D. Johnston, S. M. Kent, S. J. Kleinman, G. R. Knapp, J. Krzesinski, D. Long, E. H. Neilsen, Jr., A. Nitta, C. Loomis, R. H. Lupton, S. Roweis, S. A. Snedden, M. A. Strauss, and D. L. Tucker, *An Improved Photometric Calibration of the Sloan Digital Sky Survey Imaging Data*, *ApJ* **674** (Feb., 2008) 1217–1233, [[astro-ph/0703454](#)].
- [16] L. Knox, *Determination of inflationary observables by cosmic microwave background anisotropy experiments*, *Physical Review D*. **52** (Oct., 1995) 4307–4318, [[astro-ph/9504054](#)].
- [17] M. P. Hobson and J. Magueijo, *Observability of secondary Doppler peaks in the cosmic microwave background radiation power spectrum by experiments with small fields*, *MNRAS* **283** (Dec., 1996) 1133–1146, [[astro-ph/9603064](#)].
- [18] P. J. E. Peebles, *Statistical Analysis of Catalogs of Extragalactic Objects. I. Theory*, *ApJ* **185** (Oct., 1973) 413–440.
- [19] P. J. E. Peebles, *The large-scale structure of the universe*. Princeton, N.J., Princeton University Press, 435 p., 1980.
- [20] N. Afshordi, *Integrated Sachs-Wolfe effect in cross-correlation: The observer’s manual*, *Physical Review D*. **70** (Oct., 2004) 083536, [[astro-ph/0401166](#)].

- [21] A. Faltenbacher, A. Finoguenov, and N. Drory, *The Halo Mass Function Conditioned on Density from the Millennium Simulation: Insights into Missing Baryons and Galaxy Mass Functions*, *ApJ* **712** (Mar., 2010) 484–493, [[arXiv:1002.0844](#)].
- [22] H. J. Mo, X. Yang, F. C. van den Bosch, and Y. P. Jing, *The dependence of the galaxy luminosity function on large-scale environment*, *MNRAS* **349** (Mar., 2004) 205–212, [[astro-ph/0310147](#)].
- [23] D. J. Croton, G. R. Farrar, P. Norberg, M. Colless, J. A. Peacock, I. K. Baldry, C. M. Baugh, J. Bland-Hawthorn, T. Bridges, R. Cannon, et al., *The 2dF Galaxy Redshift Survey: luminosity functions by density environment and galaxy type*, *MNRAS* **356** (Jan., 2005) 1155–1167, [[astro-ph/0407537](#)].
- [24] A. Mecurio, P. Merluzzi, C. P. Haines, R. J. Smith, G. Busarello, and J. R. Lucey, *NIR luminosity functions and stellar mass functions of galaxies in the Shapley supercluster environment.*, *Memorie della Societa Astronomica Italiana Supplementi* **19** (2012) 237.
- [25] M. Bartelmann and P. Schneider, *Weak gravitational lensing*, *Physics Reports* **340** (Jan., 2001) 291–472, [[astro-ph/9912508](#)].
- [26] T. J. Broadhurst, A. N. Taylor, and J. A. Peacock, *Mapping cluster mass distributions via gravitational lensing of background galaxies*, *ApJ* **438** (Jan., 1995) 49–61, [[astro-ph/9406052](#)].
- [27] P. Zhang, M. Liguori, R. Bean, and S. Dodelson, *Probing Gravity at Cosmological Scales by Measurements which Test the Relationship between Gravitational Lensing and Matter Overdensity*, *Physical Review Letters* **99** (Oct., 2007) 141302, [[arXiv:0704.1932](#)].
- [28] E. Bertschinger, *One gravitational potential or two? Forecasts and tests*, *Royal Society of London Philosophical Transactions Series A* **369** (Dec., 2011) 4947–4961, [[arXiv:1111.4659](#)].
- [29] D. Larson, J. Dunkley, G. Hinshaw, E. Komatsu, M. R.olta, C. L. Bennett, B. Gold, M. Halpern, R. S. Hill, N. Jarosik, et al., *Seven-year Wilkinson Microwave Anisotropy Probe (WMAP) Observations: Power Spectra and WMAP-derived Parameters*, *ApJ. S* **192** (Feb., 2011) 16, [[arXiv:1001.4635](#)].
- [30] D. J. Eisenstein and W. Hu, *Baryonic Features in the Matter Transfer Function*, *ApJ* **496** (Mar., 1998) 605–+, [[astro-ph/9709112](#)].
- [31] M. Tegmark, M. R. Blanton, M. A. Strauss, F. Hoyle, D. Schlegel, R. Scoccimarro, M. S. Vogeley, D. H. Weinberg, I. Zehavi, A. Berlind, et al., *The Three-Dimensional Power Spectrum of Galaxies from the Sloan Digital Sky Survey*, *ApJ* **606** (May, 2004) 702–740, [[astro-ph/0310725](#)].
- [32] R. de Putter, O. Mena, E. Giusarma, S. Ho, A. Cuesta, H.-J. Seo, A. Ross, M. White, D. Bizyaev, H. Brewington, et al., *New Neutrino Mass Bounds from Sloan Digital Sky Survey III Data Release 8 Photometric Luminous Galaxies*, *ArXiv e-prints* (Jan., 2012) [[arXiv:1201.1909](#)].
- [33] A. G. Sanchez, C. G. Scoccola, A. J. Ross, W. Percival, M. Manera, F. Montesano, X. Mazzalay, A. J. Cuesta, D. J. Eisenstein, E. Kazin, et al., *The clustering of galaxies in the SDSS-III Baryon Oscillation Spectroscopic Survey: cosmological implications of the large-scale two-point correlation function*, *ArXiv e-prints* (Mar., 2012) [[arXiv:1203.6616](#)].
- [34] R. B. Tully and J. R. Fisher, *A new method of determining distances to galaxies*, *A&A* **54** (Feb., 1977) 661–673.
- [35] C. M. Springob, C. Magoulas, R. Proctor, M. Colless, D. H. Jones, C. Kobayashi, L. Campbell, J. Lucey, and J. Mould, *The 6dF Galaxy Survey: stellar population trends across and through the Fundamental Plane*, *MNRAS* (Jan., 2012) 2337, [[arXiv:1110.1916](#)].
- [36] M. Davis, A. Nusser, K. L. Masters, C. Springob, J. P. Huchra, and G. Lemson, *Local gravity*

versus local velocity: solutions for β and non-linear bias, *MNRAS* **413** (June, 2011) 2906–2922, [[arXiv:1011.3114](#)].

- [37] M. Bilicki, M. Chodorowski, T. Jarrett, and G. A. Mamon, *Is the Two Micron All Sky Survey Clustering Dipole Convergent?*, *ApJ* **741** (Nov., 2011) 31, [[arXiv:1102.4356](#)].
- [38] Z. Ivezić, J. A. Tyson, E. Acosta, R. Allsman, S. F. Anderson, J. Andrew, R. Angel, T. Axelrod, J. D. Barr, A. C. Becker, et al., *LSST: from Science Drivers to Reference Design and Anticipated Data Products*, *ArXiv e-prints* (May, 2008) [[arXiv:0805.2366](#)].